Pacific Exploratory Mission in the tropical Pacific: PEM-Tropics A, August-September 1996

JOURNAL OF GEOPHYSICAL RESEARCH, VOL. 104, NO. D5, PAGES 5567–5583, MARCH 20, 1999

Pacific Exploratory Mission in the tropical Pacific: PEM-Tropics A, August–September 1996

J. M. Hoell,[1] D. D. Davis,[2] D. J. Jacob,[3] M. O. Rodgers,[2] R. E. Newell,[4] H. E. Fuelberg,[5] R. J. McNeal,[6] J. L. Raper,[1] and R. J. Bendura[1]

Abstract. The NASA Pacific Exploratory Mission to the Pacific tropics (PEM-Tropics) is the third major field campaign of NASA's Global Tropospheric Experiment (GTE) to study the impact of human and natural processes on the chemistry of the troposphere over the Pacific basin. The first two campaigns, PEM-West A and B were conducted over the northwestern regions of the Pacific and focused on the impact of emissions from the Asian continent. The broad objectives of PEM-Tropics included improving our understanding of the oxidizing power of the tropical atmosphere as well as investigating oceanic sulfur compounds and their conversion to aerosols. Phase A of the PEM-Tropics program, conducted between August–September 1996, involved the NASA DC-8 and P-3B aircraft. Phase B of this program is scheduled for March/April 1999. During PEM-Tropics A, the flight tracks of the two aircraft extended zonally across the entire Pacific Basin and meridionally from Hawaii to south of New Zealand. Both aircraft were instrumented for airborne measurements of trace gases and aerosols and meteorological parameters. The DC-8, given its long-range and high-altitude capabilities coupled with the lidar instrument in its payload, focused on transport issues and ozone photochemistry, while the P-3B, with its sulfur-oriented instrument payload and more limited range, focused on detailed sulfur process studies. Among its accomplishments, the PEM-Tropics A field campaign has provided a unique set of atmospheric measurements in a heretofore data sparse region; demonstrated the capability of several new or improved instruments for measuring OH, H_2SO_4, NO, NO_2, and actinic fluxes; and conducted experiments which tested our understanding of HO_x and NO_x photochemistry, as well as sulfur oxidation and aerosol formation processes. In addition, PEM-Tropics A documented for the first time the considerable and widespread influence of biomass burning pollution over the South Pacific, and identified the South Pacific Convergence Zone as a major barrier for atmospheric transport in the southern hemisphere.

1. Introduction

During the early part of this decade, NASA through its Earth Sciences Program initiated the Pacific Exploratory Missions (PEM) to improve scientific understanding of human influences on the tropospheric chemistry over the Pacific Ocean. The PEM studies were conducted as part of NASA's Global Tropospheric Experiment (GTE) and, to date, have consisted of three airborne campaigns. PEM-West A and B were conducted over the northwestern Pacific during September–October 1992 (PEM-West A [*Hoell et al.*, 1996]) and February–March 1994 (PEM-West B [*Hoell et al.*, 1997]) to study Asian outflow during contrasting meteorological conditions. The third, PEM-Tropics A, was conducted during August–September 1996 and focused on the southern tropical regions of the Pacific Ocean, extending zonally across the entire Pacific basin and meridionally from Hawaii to south of New Zealand. A fourth campaign, PEM-Tropics B, is scheduled for March/April 1999. Like PEM-West A and B, the combined PEM-Tropics A and B campaigns will provide observations during contrasting seasons (i.e., dry versus wet). This paper describes the experimental design of the PEM-Tropics A campaign and summarizes some of the results given in the companion papers in this issue.

One of the most important issues in global tropospheric chemistry is the sensitivity of the oxidizing power of the troposphere to human influence. From the perspective of global tropospheric chemistry, the Pacific basin is a very large chemical reaction vessel. From Peru to Borneo, it stretches 17,700 km in the east-west direction; the distance from the Antarctic ice shelf to Alaska is 13,300 km. The Pacific basin covers 35% of the total surface area of the Earth, and 50% of the ocean surface. Since much of the Pacific basin is far removed from continental influences, observations in this region can provide sensitive indicators of the global-scale impact of human activity on the oxidizing power of the troposphere.

There also is a need to improve our understanding of atmospheric sulfur chemistry over the Pacific. Sulfate aerosols affect the Earth's radiative balance through direct backscattering of solar radiation and indirectly as cloud condensation nuclei (CCN). CCN, themselves products of aerosol growth processes, are believed to originate through nucleation processes involving gas phase H_2SO_4 that is produced from the oxidation of SO_2 by OH. Sulfate and SO_2 over the Pacific may originate from a number of

[1]NASA Langley Research Center, Hampton, Virginia.
[2]Georgia Institute of Technology, Atlanta.
[3]Harvard University, Cambridge, Massachussetts.
[4]Massachusetts Institute of Technology, Cambridge, Massachussetts.
[5]Florida State University, Tallahassee.
[6]NASA Headquarters, Washington, D.C.

Paper number 1998JD100074.
0148-0227/99/1998JD100074$09.00

sources including long-range transport of anthropogenic pollution, marine biogenic releases of dimethlysulfide (DMS), and volcanic emissions. The relative contributions of these sources over different regions of the Pacific are still poorly known, representing a serious limitation in our ability to evaluate the role of sulfur in global climate change.

Prior to the PEM campaigns, there were little chemical data for the southern tropical Pacific region. The Global Atmospheric Measurements Experiment on Tropospheric Aerosols and Gases (GAMETAG) aircraft missions in 1977 and 1978 [*Davis*, 1980] provided some early data over the western part of the Pacific. However, these campaigns were restricted by the low ceiling and limited endurance of the aircraft, and also by the instrumentation available at the time. The more recent STRATOZ III [*Drummond et al.*, 1988] and PEM-West A and B missions have provided detailed data along the South American and Asian rims of the southern Pacific basin, respectively and ozonesonde and CO measurements have been made from island sites during the Sea-Air Exchange (SEAREX) program. Even so, there were virtually no data for the southeast quadrant of the Pacific basin extending from the international dateline to the South American coast. The PEM-Tropics A observations (and those from the forthcoming PEM-Tropics B campaign) provide an extensive set of atmospheric measurements in a heretofore data sparse region. Data from this mission (e.g., airborne chemical measurements, meteorological and ozonesonde observations, and model products), along with data from all previous GTE field campaigns, have been archived in the Langley Distributed Active Archive Center (http://eosweb.larc.nasa.gov) and/or on the GTE Home Page at http://www-gte.larc.nasa.gov.

2. Implementation of the PEM-Tropics Campaign

The major objectives of PEM-Tropics (phases A and B) are to provide baseline data over the southern Pacific Ocean for gases important in controlling the oxidizing power of the atmosphere, including O_3, H_2O, NO, CO_x, and hydrocarbons, to improve scientific understanding of the factors controlling the concentrations of these gases, and to assess the resulting sensitivity of the oxidizing power of the atmosphere to anthropogenic and natural perturbations. In addition, PEM-Tropics A had three secondary objectives: (1) to survey the concentrations of aerosol precursors and ultrafine aerosol particles over the southern Pacific basin; (2) to improve our understanding of sulfur gas-to-particle formation over the region; and (3) to provide detailed latitude-altitude transects of long-lived gases for the evaluation of global tropospheric models.

To address these objectives, NASA, through a competitive process (Announcement of Opportunity), selected investigators who provided measurements and/or model analyses during PEM-Tropics A. The PEM-Tropics Science Team consisted of the Principal Investigator(s) from each investigative group. The Mission Scientists and Mission Meteorologists, also competitively selected, led the science team in developing the detailed design of the PEM-Tropics A campaign. Tables 1a and 1b list the DC-8 and P-3B aircraft investigations, respectively, with the salient measurement characteristics for each instrument. Table 2 lists the meteorological and modeling investigations, along with the Mission Meteorologists and Scientists. The aircraft instrumentation layout is included in Figures 1a and 1b for the DC-8 and P-3B, respectively.

The NASA DC-8 aircraft has a nominal ceiling of 12 km, a cruising speed of 800 km/h, and, as configured during PEM-Tropics A, a 10 hour flight endurance. The P-3B aircraft has a nominal ceiling of 8 km, a cruising speed of 500 km/h, and, as configured in PEM-Tropics A, a nominal 8 hour endurance. These differing characteristics, coupled with the instrument payload of each aircraft, favored use of the DC-8 for long-range transport studies and high-altitude observations and favored the P-3B for lower-altitude, process-oriented studies. The differential absorption lidar (DIAL) aboard the DC-8 provided vertical profiles of ozone and aerosol above and below the aircraft [*Browell et al.*, 1996], thereby enhancing transport studies conducted by the DC-8. The DIAL profiles provided a two-dimensional perspective of the structure of the troposphere in which the in situ measurements aboard the DC-8, and in some cases the P-3B, were recorded. The DIAL profiles also provided real-time guidance for adjusting the DC-8 flight tracks to exploit interesting measurement opportunities encountered in-flight.

The P-3B instrument payload included measurements of a unique suite of sulfur species [DMS, SO_2, methane sulfonic acid (MSA) [gas], H_2SO_4 [gas], non-sea-salt sulfate (NSS), and methane sulfonate (MS)], along with aerosol composition and size distributions, including ultrafine particles. These measurements, combined with the capability for reliable observations of OH, via the Chemical Ionization Mass Spectrometry (CIMS) technique [*Eisele and Tanner*, 1991], provided a unique opportunity for the focused sulfur process studies that were conducted by the P-3B.

The broad design of the PEM-Tropics A campaign employed a series of flights from remote operational sites in the South Pacific basin. Figures 2a and 2b show these sites, along with flight tracks of the DC-8 (Figure 2a) and the P-3B (Figure 2b) aircraft. The flight numbers in Figure 2 are keyed to Tables 3a and 3b in which the major focus of each flight is summarized. As part of the overall design of PEM-Tropics, measurements obtained from the NASA DC-8 and P-3B during the intensive deployment period were augmented by ozonesonde observations from operational launch sites at Easter Island, and Lauder, New Zealand (also shown in Figure 2), and by stations established by the GTE Project at Papeete, Tahiti, and American Samoa. Figure 2 also shows the ozonesonde release site on Fiji which was established by the GTE project in August 1997 to support the PEM-Tropics B mission. Ozonesondes at all the sites, except Fiji, were released at a rate of one per week, beginning in August 1995, approximately 1 year prior to the aircraft campaign in 1996. Releases at all sites are scheduled to continue through October 1999, to encompass the upcoming PEM-Tropics B mission, and a final survey of the dry season period. During the aircraft deployment periods, the sites established by GTE and the Lauder station increased their launch rate to two per week. It is anticipated that the ozonesonde data from Fiji and Samoa will provide an indicator of the seasonal changes in the gradients of trace gases that were observed to exist across the South Pacific Convergence Zone (SPCZ) during PEM-Tropics A [*Gregory et al.*, this issue].

Meteorological support for real-time flight planning and post-mission analyses to assist in coupling air mass transport and chemistry is a critical element of GTE field campaigns. Meteorological support for in-field flight planning during PEM-Tropics A was provided by a Mission Meteorologist stationed with each aircraft, with supporting activities at the Massachusetts Institute of Technology (MIT) and Florida State University (FSU). Meteo France also provided significant support by allowing direct access to European Centre for Medium-Range Weather Forecasts (ECMWF) gridded data and by providing valuable consultations at their Papeete, Tahiti, facilities. Satellite images received and stored at MIT, along with derived products from FSU and MIT

Table 1a. PEM-Tropics A Nominal Measurement Characteristics of Instruments on the DC-8

Species Parameter	Investigator	Technique	Averaging Time	Accuracy	Nominal Precision	Nominal Lod
NO	J. Bradshaw	TP-LIF	9.6 s (ranging from 0.22–556 s)	62.6 ±63.3 pptv (1)	6.0 ±5.5 pptv (1)	0.89 ±0.89 (ranging from 0.14–5.09 pptv)
NO_2	J. Bradshaw	PF/TP-LIF	3 min	12 ±16 pptv (2)	2.6 ±2.24 pptv (2)	4.4 ±3.4 pptv
O_3	G. Gregory	chemiluminescence	0.5 s	3% or 2 ppbv	2% 0r 1 ppbv	1 ppbv
CO	G. Sachse	TDL	5 s	1%	1 ppbv or 1%	NA
CH_4	G. Sachse	TDL	5 s	1%	3 ppbv	NA
H_2O vapor	G. Sachse	diode laser specrometer	0.05 s	±10%	±2% or 0.2 ppm	0.2 ppm
CO_2	S. Vay	NDIR	5 s	300 ppbv	100 ppbv	NA
Remote O_3 Profile	E. Browell	UV DIAL	5 min (3)	10% or 2 ppbv	5% or 1 ppbv	<5 ppbv
Remote aerosol profile	E. Browell	UV DIAL (visible)	2 s (4)	10%	1%	NA
H_2O	J. Barrick	cryogenic chilled mirror hygrometer	1 s	±0.5–1.0°C	±0.2°C	−100°C
H_2O_2	B. Heikes	grab samples/HPLC	2.5 min	±30%	10 pptv	15 pptv
CH_3OOH	B. Heikes	grab samples/HPLC	2.5 min	±30%	15 pptv	25 pptv
Condensation nuclei (CN)	B. Anderson	butanol CN counter	10 s	10%	5%	25.4 (ultra-fine)-0.547 (fine)
DMS	A. Bandy	GC/GMS	3–5 min	<10%	1 pptv	2
SO_2	A. Bandy	GC/GMS	3–5 mın	<10%	1pptv	1
PAN	H. Singh	GC/ECD	150 s	±20%	±10% or ±1 pptv	1
PPN	H. Singh	GC/ECD	150 s	±30%	±20% or ±1 pptv	1
C_2Cl_4	H. Singh	GC/ECD	150 s	±10%	±10% or ±1 pptv	0.5
Methyl_Nitrate	H. Singh	GC/ECD	150 s	±20%	±10%	1
Ethyl/i-Propyl_Nitrate	H. Singh	GC/ECD	150 s	±20%	±10%	1
HNO_3	R. Talbot	aqueous scrub/IC	4–8 min	30–35% (5)	30–35%	<20 pptv
HCOOH	R. Talbot	aqueous scrub/IC	4–8 min	15%	15%	10–31 pptv
CH_3COOH	R. Talbot	aqueous scrub/IC	4–8 min	20%	20%	10–31 pptv
Chloride	R. Talbot	filter/IC	10–20 min	30%	35%	20
Nitrate	R. Talbot	filter/IC	10–20 min	20%	10%	10
Oxalate	R. Talbot	filter/IC	10–20 min	10%	15%	1
Sulfate	R. Talbot	filter/IC	10–20 min	13%	10%	3.5
Methylsulfonate	R. Talbot	filter/IC	10–20 min	10%	15%	0.5
Ammonium	R. Talbot	filter/IC	10–20 min	15%	15%	20
Sodium	R. Talbot	filter/IC	10–20 min	35%	35%	50
Potassium	R. Talbot	filter/IC	10–20 min	20%	20%	15
Magnesium	R. Talbot	filter/IC	10–20 min	10%	10%	6.5
Calcium	R. Talbot	filter/IC	10–20 mın	15%	15%	15
Be-7	R. Talbot	filter/gama spectroscopy	10–20 min	20%	15%	100 fCi/scm
Pb-210	R. Talbot	filter/alpha spectroscopy	10–20 min	20%	10%	0.1 fCi/scm

Table 1a. (continued)

Species Parameter	Investigator	Technique	Averaging Time	Accuracy	Nominal Precision	Nominal Lod
CFC-12	D. Blake	grab sample/GC	10–75 s	2%	0.7%	1.0
CFC-11	D. Blake	grab sample/GC	10–75 s	2%	0.8%	3
CFC-113	D. Blake	grab sample/GC	10–75 s	2%	1.4%	3
CFC-114	D. Blake	grab sample/GC	10–75 s	5%	1.5%	1
HCFC-22	D. Blake	grab sample/GC	10–75 s	5%	1.5%	10
H-1301	D. Blake	grab sample/GC	10–75 s	5%	2%	0.1
H-1211	D. Blake	grab sample/GC	10–75 s	5%	2%	0.1
H-2402	D. Blake	grab sample/GC	10–75 s	5%	5%	0.1
CH_3Cl	D. Blake	grab sample/GC	10–75 s	5%	2%	100
CH_3Br	D. Blake	grab sample/GC	10–75 s	5%	4%	1
CH_3I	D. Blake	grab sample/GC	10–75 s	10%	5–10% (6)	0.05
$CHCl_3$	D. Blake	grab sample/GC	10–75 s	5%	2%	2
CH_3CCl_3	D. Blake	grab sample/GC	10–75 s	5%	1%	3
CCl_4	D. Blake	grab sample/GC	10–75 s	5%	1%	3
C_2Cl_4	D. Blake	grab sample/GC	10–75 s	10%	1–5% (6)	0.05
$CHBrCl_2$	D. Blake	grab sample/GC	10–75 s	10–20% (6)	5–10% (6)	0.05
CH_2Br_2	D. Blake	grab sample/GC	10–75 s	10–20% (6)	5–10% (6)	0.4
$CHClBr_2$	D. Blake	grab sample/GC	10–75 s	10–20% (6)	5–10% (6)	0.005
$CHBr_3$	D. Blake	grab sample/GC	10–75 s	10–20% (6)	5–10% (6)	0.005
Methyl nitrate	D. Blake	grab sample/GC	10–75 s	10–20% (6)	5–10% (6)	0.05
Ethyl nitrate	D. Blake	grab sample/GC	10–75 s	10–20% (6)	5–10% (6)	0.05
1-Propyl nitrate	D. Blake	grab sample/GC	10–75 s	10–20% (6)	5–10% (6)	0.05
2-Propyl nitrate	D. Blake	grab sample/GC	10–75 s	10–20% (6)	5–10% (6)	0.05
2-Butyl nitrate	D. Blake	grab sample/GC	10–75 s	10–20% (6)	5–10% (6)	0.05
Ethane	D. Blake	grab sample/GC	10–75 s	5%	1% or 2 pptv	3
Ethene	D. Blake	grab sample/GC	10–75 s	10%	3 pptv	2
Propane	D. Blake	grab sample/GC	10–75 s	5%	1% or 2 pptv	3
Propene	D. Blake	grab sample/GC	10–75 s	10%	3 pptv	2
i-Butane	D. Blake	grab sample/GC	10–75 s	5%	1% or 2 pptv	2
n-Butane	D. Blake	grab sample/GC	10–75 s	5%	1% or 2 pptv	2
Ethyne	D. Blake	grab sample/GC	10–75 s	5%	1% or 2 pptv	2
Isoprene	D. Blake	grab sample/GC	10–75 s	10%	3% or 3 pptv	2
n-Pentane	D. Blake	grab sample/GC	10–75 s	5%	1% or 2 pptv	2
i-Pentane	D. Blake	grab sample/GC	10–75 s	5%	1% or 2 pptv	2
CH_3ONO_2	E. Atlas	(7)	10–75 s	10–20% (6)	5–10% (6)	< 0.1 ppt (8)
$C_2H_5ONO_2$	E. Atlas	(7)	10–75 s	10–20% (6)	5–10% (6)	< 0.1 ppt (8)
$i\text{-}C_3H_7ONO_2$	E. Atlas	(7)	10–75 s	10–20% (6)	5–10% (6)	< 0.1 ppt (8)
$n\text{-}C_3H_7ONO_2$	E. Atlas	(7)	10–75 s	10–20% (6)	5–10% (6)	< 0.1 ppt (8)
$2\text{-}C_4H_9ONO_2$	E. Atlas	(7)	10–75 s	10–20% (6)	5–10% (6)	< 0.1 ppt (8)
$3\text{-}CH_3\text{-}2\text{-}C_4H_9ONO_2$	E. Atlas	(7)	10–75 s	10–20% (6)	5–10% (6)	< 0.1 ppt (8)

Table 1a. (continued)

Species Parameter	Investigator	Technique	Averaging Time	Accuracy	Nominal Precision	Nominal Lod
$3\text{-}C_5H_{11}ONO_2$	E. Atlas	(7)	10–75 s	10–20% (6)	5 –10% (6)	< 0.1 ppt (8)
$2\text{-}C_5H_{11}ONO_2$	E. Atlas	(7)	10–75 s	10–20% (6)	5–10% (6)	< 0.1 ppt (8)
CH_2C_{12}	E. Atlas	(7)	10–75 s	10–20% (6)	5–10% (6)	<1 ppt (8)
$HCFC1_41B$	E. Atlas	(7)	10–75 s	10–20% (6)	5–10% (6)	< 0.1 ppt (8)
$HCFC1_42B$	E. Atlas	(7)	10–75 s	10–20% (6)	5–10% (6)	< 0.1 ppt (8)
HFC134A	E. Atlas	(7)	10–75 s	10–20% (6)	5–10% (6)	< 0.1 ppt (8)
CH_2Br_2	E. Atlas	(7)	10–75 s	10–20% (6)	5–10% (6)	< 0.1 ppt (8)
$CHBrCl_2$	E. Atlas	(7)	10–75 s	10–20% (6)	5–10% (6)	< 0.1 ppt (8)
$CHBr_2Cl$	E. Atlas	(7)	10–75 s	10–20% (6)	5–10% (6)	< 0.1 ppt (8)
$CHBr_3$	E. Atlas	(7)	10–75 s	10–20% (6)	5–10% (6)	< 0.1 ppt (8)
$J(NO_2)$ zenith and nadir	J. Barrick	hemispherical radiometer	1 s	±5%	±1%	NA
Nadir and zenith spectroradiometer	R. Shetter	actinic flux spectroradiometry	30 s	±5%	±5%	(9)
Aircraft ephemeris data	DC-8	GPS	1 s	±25m	±25m	1m
Surface temperature	DC-8	pyrometer	1 s	±0.5°C	±0.2°C	–50°C
Dew point	DC-8	2 and 3 stage frost point hygrometer	1 s	±0.5–1.0 °C	±0.2°C	–100°C

Notes: (1) Total uncertainty in range 0.3 to 53 pptv is 12.0±7.3 pptv. (2) Total uncertainty in range 0.3 to 52 pptv is 3.7 ±4.0 pptv. (3) The vertical resolution is 300 m. Horizontal resolution is 5 min (approximately 70 km). The data are archived at a vertical sampling interval of 300 m and a horizontal sampling interval of 60 s (approximately 14 km). (4) The vertical averaging interval is 60 m. Horizontal averaging interval is 2 seconds (approximately 470 m). The data are archived at a vertical sampling interval of 90 m and a horizontal sampling interval of 60 s (approximately 14 km). (5) Accuracy is 30–35% at LOD, 20% at 25–100 pptv, 15% at >100 pptv. (6) Higher uncertainty for molecules with mixing ratios in the 0.001–0.1 pptv range. (7) Analysis was performed on whole air samples aquired by D. Blake. The analytical technique was gas chromatography with mass spectrometric (EI and NICI) detection. (8) For some molecules with mixing ratios near the limit of detection, null values were used to replace zero values for reasons of analytical problems or to indicate limit of detection. (9) The given lower limits of detection are the 2-sigma values of the flight period 0250–0310 on October 6 (during total darkness).

Table 1b. PEM-Tropics A Nominal Measurement Characteristics of Instruments on the P3-B

Species Parameter	Investigator	Technique	Averaging Time	Accuracy	Nominal Precision	Nominal Lod
NO	M. Carroll	chemiluminescence	60 s	7% (1)	20% (1)(2)	4 pptv (3)
O_3	M. Carroll	chemiluminescence	1 s	7% (1)(4)	8% (1)	<100 pptv
CO	G. Sachse	diode laser specrometer	5 s	2%	1 ppbv or 1%	NA
CH_4	G. Sachse	diode laser specrometer	5 s	1%	1 ppbv	NA
CO_2	B. Anderson	NDIR	5 s	300 ppbv	100 ppbv	NA
H_2O_2	B. Heikes	grab samples/HPLC	5 min	±30%	10 pptv	15 pptv
CH_3OOH	B. Heikes	grab samples/HPLC	5 min	±30%	15 pptv	25 pptv
OH	F. Eisele	CIMS	30 s	(5)	20–40%	500,000/cm^3
H_2SO_4	F. Eisele	CIMS	30 s	(5)	20–40%	200,000/cm^3
MSA	F. Eisele	CIMS	30 s	factor of 2	20–40%	500,000/cm^3
DMS	A. Bandy	GC/MS	30 s	NA	1 pptv	2 pptv
SO_2	A. Bandy	GC/MS	30 s	NA	1 pptv	1 pptv
MS	B. Huebert	filter sampling	15–70 min	NA	NA	NA
SO_4	B. Huebert	filter sampling	15–70 min	NA	NA	NA
Na	B. Huebert	filter sampling	15–70 min	NA	NA	NA
NH_4	B. Huebert	filter sampling	15–70 min	NA	NA	NA
NSS	B. Huebert	filter sampling	15–70 min	NA	NA	NA
HNO_3	B. Huebert	filter sampling	15–70 min	NA	NA	NA
Total NO_3	B. Huebert	filter sampling	15–70 min	NA	NA	NA
NH_4/NSS ratio	B. Huebert	filter sampling	15–70 min	NA	NA	NA
Total scatter	A. Clarke	nephelometer	15 s	±2E–7 m^{-1}	±1E–7 m^{-1}	2E–7 m^{-1}
Submicron scatter	A. Clarke	nephelometer	15 s	±2E–7 m^{-1}	±1E–7 m^{-1}	2E–7 m^{-1}
Ultrafine CN (3025)	A. Clarke	CN counter	15 s	5%	5%	particles/cm^3
CN (3010)	A. Clarke	CN counter	15 s	5%	5%	particles/cm^3
CN (3760 at 30°C)	A. Clarke	CN counter	15 s	5%	5%	particles/cm^3
CN (3760 at 300°C)	A. Clarke	CN counter	15 s	5%	5%	particles/cm^3
Dry CN, surface area volume	A. Clarke	RDMA	40 s	20%	5%	.007<Dp<.148 Fm
Dry CN, surface area volume	A. Clarke	OPC	60 s	15%	5%	0.148<Dp<6 Fm
H-1301	D. Blake	grab samples/GC	10–75 s	5%	2%	0.1
H-1211	D. Blake	grab samples/GC	10–75 s	5%	2%	0.1
H-2404	D. Blake	grab samples/GC	10–75 s	5%	5%	0.1
HCFC-22	D. Blake	grab samples/GC	10–75 s	5%	1.5%	10
F-12	D. Blake	grab samples/GC	10–75 s	2%	0.7%	1.0
F-11	D. Blake	grab samples/GC	10–75 s	2%	0.8%	3
F-112	D. Blake	grab samples/GC	10–75 s	5%	3%	2 pptv
F-113	D. Blake	grab samples/GC	10–75 s	2%	1.4%	3
F-114	D. Blake	grab samples/GC	10–75 s	5%	1.5%	1

Table 1b. (continued)

Species Parameter	Investigator	Technique	Averaging Time	Accuracy	Nominal Precision	Nominal Lod
CH_3Cl	D. Blake	grab samples/GC	10–75 s	5%	2%	100
MeBr	D. Blake	grab samples/GC	10–75 s	5%	5%	1 pptv
CH_3I	D. Blake	grab samples/GC	10–75 s	10%	5–10% (6)	0.05
$CHCl_3$	D. Blake	grab samples/GC	10–75 s	5%	2%	2
$MeCCl_3$	D. Blake	grab samples/GC	10–75 s	NA	5%	2 pptv
CCl_4	D. Blake	grab samples/GC	10–75 s	5%	1%	3
C_2Cl_4	D. Blake	grab samples/GC	10–75 s	10%	1–5% (6)	0.05
$CHCl_2Br$	D. Blake	grab samples/GC	10–75 s	10–20% (6)	5–10% (6)	0.05
CH_2Br_2	D. Blake	grab samples/GC	10–75 s	10–20% (6)	5–10% (6)	0.4
$CHClBr_2$	D. Blake	grab samples/GC	10–75 s	10–20% (6)	5–10% (6)	0.005
$CHBr_3$	D. Blake	grab samples/GC	10–75 s	10–20% (6)	5–10% (6)	0.05
$MeONO_2$	D. Blake	grab samples/GC	10–75 s	10–20% (6)	5–10% (6)	0.05
$EtONO_2$	D. Blake	grab samples/GC	10–75 s	10–20% (6)	5–10% (6)	0.05
1-$PrONO_2$	D. Blake	grab samples/GC	10–75 s	10–20% (6)	5–10% (6)	0.05
2-$PrONO_2$	D. Blake	grab samples/GC	10–75 s	10–20% (6)	5–10% (6)	0.05
2-$BuONO_2$	D. Blake	grab samples/GC	10–75 s	10–20% (6)	5–10% (6)	0.05
Ethane	D. Blake	grab samples/GC	10–75 s	5%	1% or 2 pptv	3
Ethene	D. Blake	grab samples/GC	10–75 s	10%	3 pptv	2
Ethyne	D. Blake	grab samples/GC	10–75 s	5%	1% or 2 pptv	2
Propane	D. Blake	grab samples/GC	10–75 s	5%	1% or 2 pptv	3
Propene	D. Blake	grab samples/GC	10–75 s	10%	3 pptv	2
i-Butane	D. Blake	grab samples/GC	10–75 s	5%	1% or 2 pptv	2
n-Butane	D. Blake	grab samples/GC	10–75 s	5%	1% or 2 pptv	2
i-Pentane	D. Blake	grab samples/GC	10–75 s	5%	1% or 2 pptv	2
n-Pentane	D. Blake	grab samples/GC	10–75 s	5%	1% or 2 pptv	2
Isoprene	D. Blake	grab samples/GC	10–75 s	10%	3% or 3 pptv	2
CH_3ONO_2	E. Atlas	(7)	10–75 s	10–20% (6)	5–10 % (6)	<0.1 ppt
$C_2H_5ONO_2$	E. Atlas	(7)	10–75 s	10–20% (6)	5–10 % (6)	<0.1 ppt
i-$C_3H_7ONO_2$	E. Atlas	(7)	10–75 s	10–20% (6)	5–10 % (6)	<0.1 ppt
n-$C_3H_7ONO_2$	E. Atlas	(7)	10–75 s	10–20% (6)	5–10 % (6)	<0.1 ppt
2-$C_4H_9ONO_2$	E. Atlas	(7)	10–75 s	10–20% (6)	5–10 % (6)	<0.1 ppt
3-CH_3-2-$C_4H_9ONO_2$	E. Atlas	(7)	10–75 s	10–20% (6)	5–10 % (6)	<0.1 ppt
3-$C_5H_{11}ONO_2$	E. Atlas	(7)	10–75 s	10–20% (6)	5–10 % (6)	<0.1 ppt
2-$C_5H_{11}ONO_2$	E. Atlas	(7)	10–75 s	10–20% (6)	5–10 % (6)	<0.1 ppt
CH_2Cl_2	E. Atlas	(7)	10–75 s	10–20% (6)	5–10 % (6)	< 1 ppt
HCFC141B	E. Atlas	(7)	10–75 s	10–20% (6)	5–10 % (6)	<0.1 ppt
HCFC142B	E. Atlas	(7)	10–75 s	10–20% (6)	5–10 % (6)	<0.1 ppt
HFC134A	E. Atlas	(7)	10–75 s	10–20% (6)	5–10 % (6)	<0.1 ppt

Table 1b. (continued)

Species Parameter	Investigator	Technique	Averaging Time	Accuracy	Nominal Precision	Nominal Lod
CH_2Br_2	E. Atlas	(7)	10–75 s	10–20% (6)	5–10 % (6)	<0.1 ppt
$CHBrCl_2$	E. Atlas	(7)	10–75 s	10–20% (6)	5–10 % (6)	<0.1 ppt
$CHBr_2Cl$	E. Atlas	(7)	10–75 s	10–20% (6)	5–10 % (6)	<0.1 ppt
$CHBr_3$	E. Atlas	(7)	10–75 s	10–20% (6)	5–10 % (6)	<0.1 ppt
$J(NO_2)$ zenith and nadir	M. Rodgers	actinometer	60 s	NA	NA	NA
J(O1D) zenith/nadir	M. Rodgers	actinometer	60 s	NA	NA	NA
U wind component	B. Anderson	TAMMS	20 Hz	0.3 m/s	0.5 m/s	0.5 m/s
V wind component	B. Anderson	TAMMS	20 Hz	0.3 m/s	0.5 m/s	0.5 m/s
W wind component	B. Anderosn	TAMMS	20 Hz	0.1 m/s	0.2 m/s	0.2 m/s
Dew point	J. Barrick	Cryogenic chilled mirror hygrometer	1 s	±0.5–1.0°C	±0.2°C	−100°C
UV radiation/zenith and nadir	J. Barrick	Eppley radiometer	1 s	±5%	±2%	NA
Surface temperature	J. Barrick	Pyrometer	1 s	±0.5°C	±0.2°C	−50°C
Dew point	J. Barrick	2 and 3 stage frost point hygrometer	1 s	±0.5–1.0°C	±0.2°C	−100°C
Aircraft ephemeris data	J. Barrick	GPS	1 s	±25 m	±25 m	1 m

Notes: (1) Errors correspond to one sigma values. (2) Approximately half of uncertainty in precision is due to uncertainty in the artifact. (3) The detection limit corresponds to 3 times the background level. (4) During flights 4, 6, and 7, an instrument malfunction caused a systematic error of uncertain magnitude. The reported mixing ratios for ozone are lower than the real mixing ratios. Most likely the numbers are 2.5% to 20%, low. There is a small chance that the reported mixing ratios are off by more than 20% but they cannot be more than 39% low. During flight 8 a similar problem occurred. Most likely the reported mixing ratios are <1% to 5% low. There is a small chance that they can be off by more than 5% but they cannot be more than 10% low. (5) Reported error limits are +/- 42.0% for measurements made at pressures above 940 mBar, and +/– 62.0% for measurements made below 940mbar. The quoted errors are 2 sigma. A few of the later flights (14–17) were plagued with detector problems which greatly enhanced scatter in the measured data. This scatter should not significantly alter the uncertainty of the data except that a larger number of data points must be averaged to reduce the scatter in this data. The reported error for flights 14–17 is +/– a factor of 2 for measurements made at pressures above 940 mbar and an additional 20% for measurements made below 940 mbar. The increase in uncertainty at higher altitudes reflects the increased spread in the observed calibration coefficients and the increased uncertainty in the concentration of H2O at higher altitudes. (6) There is higher uncertainty for molecules with mixing ratios in the 0.001–0.1 pptv range. (7) Trace gas data are based on measurements of whole air samples collected by D. Blake. The analytical technique was gas chromatography with mass spectrometric (EI and NICI) detection. Random fluctuation in zero, measure, and artifact are all included.

Table 2. PEM-Tropics Modeling and Meteorological Studies

Principal Investigator (s)	Institution	Study
S. C. Liu	Georgia Institute of Technology	three-dimensional transport, photochemical model
J. Rodriguez and D. Sze	Atmospheric Environmental Research, Inc.	point-by-point photochemical model; steady state diurnal model and trajectory photochemical process model
D. D. Davis	Georgia Institute of Technology	instantaneous photostationary state and time dependent box model/ comission scientist/P-3B
R. E. Newell	Massachusetts Institute of Technology	chemical and meteorological analysis comission meteorologist/P-3B
Henry Fuelberg	Florida State University	real time and postmission trajectory model analysis; comission meteorologist/DC-8
Daniel Jacob	Harvard University	photochemical point model; comissoin scientist/DC-8
T. Krishnamurti	Florida State University	Florida State University global spectral model
Don Lenschow	National Center for Atmospheric Research	analysis of trace as flux measurements

(i.e., streamline and trajectory analyses at various pressure levels, potential vorticity, etc.), were transmitted to the field operations sites at Christmas Island and Easter Island using a portable high-speed satellite-telephone data link. For operations at Christmas Island, and to a lesser extent at Easter Island, this data link provided the only access to meteorological data. A combination of the satellite data link, faxed data products, and the use of local meteorological facilities were used during operations at Papeete, Tahiti, Christchurch, New Zealand, Nadi, Fiji, and Guayaquil, Ecuador.

Integration of instruments aboard the P-3B and DC-8 aircraft occurred at the NASA Wallops Flight Facility, Wallops Island, Virginia, and the NASA Ames Research Center (ARC), Moffett Field, California, respectively. The P-3B deployed approximately 1 week prior to the DC-8's departure, with transit flights to Christmas Island via ARC and Hawaii (see Table 3b). The original flight plans called for two local P-3B flights at Christmas Island; however, the P-3B experienced aircraft problems after the first local flight and returned to Hawaii for repairs. After completing integration and test flights, the DC-8 departed ARC for Tahiti via Hawaii. The DC-8 and P-3B arrived in Tahiti on the same day. During this transit flight to Tahiti, both aircraft conducted substantial vertical profiling to document interhemispheric gradients of gases, along with a coordinated low-altitude flyby of Christmas Island to document concentrations of several key constituents measured several days earlier during the P-3B's local flight from Christmas Island.

Flight operations from Tahiti included three local flights by each aircraft, followed by transit flights by both the DC-8 and the P-3B to Easter Island. Each aircraft conducted two local flights from Easter Island after which the P-3B traveled to Guayaquil, Ecuador, and the DC-8 traveled to Christchurch, New Zealand, with a stopover and local flight from Tahiti. While the DC-8 operated out of New Zealand, the P-3B conducted three local flights from Guayaquil to examine interhemispheric exchange and the primary productivity rich oceanic region near the equator prior to returning to the NASA Wallops Flight Facility. The DC-8's local flight out of Christchurch extended south to the Antarctic coast to investigate meridional gradients and the influence of transport from high latitudes on the tropical troposphere. From Christchurch, the DC-8 flew to Fiji, where three local flights were conducted, followed by the return flight to ARC via Tahiti.

3. Overview of PEM-Tropics Results

This section provides a brief synopsis of the salient results from PEM-Tropics A that are discussed in detail in the companion papers of this issue. Among its accomplishments, the PEM-Tropics A field campaign has provided a unique set of atmospheric measurements in a heretofore data sparse region; demonstrated the capability of several new or improved instruments for measuring OH, H_2SO_4, NO, and NO_2, and actinic fluxes; and conducted experiments which tested our understanding of HO_x and NO_x photochemistry, as well as for sulfur oxidation and aerosol formation processes. In addition, PEM-Tropics A documented for the first time the considerable and widespread influence of biomass burning pollution over the South Pacific, and identified the South Pacific Convergence Zone (SPCZ) as a major barrier for atmospheric transport in the southern hemisphere.

3.1. New/Improved Measurements

The DC-8 instrument payload included a new generation photo-fragmentation two-photon laser-induced fluorescence (PF-TP-LIF) instrument for measuring NO and NO_2 [*Sandholm et al.*, 1997; *J. Bradshaw et al.*, 1999]. The improved sensitivity of this instrument provided, for the first time, accurate NO measurements at sub-pptv concentrations. Further, a high flow rate sample inlet system was employed to minimize the possibility that complex nitrogen oxides would decompose in the inlet system, which had been speculated to be a problem in previous measurements of NO_2 by this group [*Crawford et al.*, 1996]. The PEM-Tropics A data showed that comparisons between measured NO/NO_2 concentration ratios and those computed with a photochemical steady state model agreed to within 30% [*Schultz et al.*, this issue]. This finding is in sharp contrast to results from the GTE PEM-West A mission, where the deviation between predicted and observed NO_2 was nearly a factor of 4 [*Crawford et al.*, 1996]. The agreement between modeled and measured NO/NO_2 is attributed to the improved sensitivity and the high flow rate inlet. Moreover, measurements by the PF-TP-LIF instrument revealed that NO concentrations in the marine boundary layer (MBL) were frequently below 1 pptv.

Also aboard the DC-8 was a new airborne actinic flux spectroradiometer [*Shetter and Müller*, this issue]. This system consisted of nadir and zenith 2 pi str radiometers, and provided

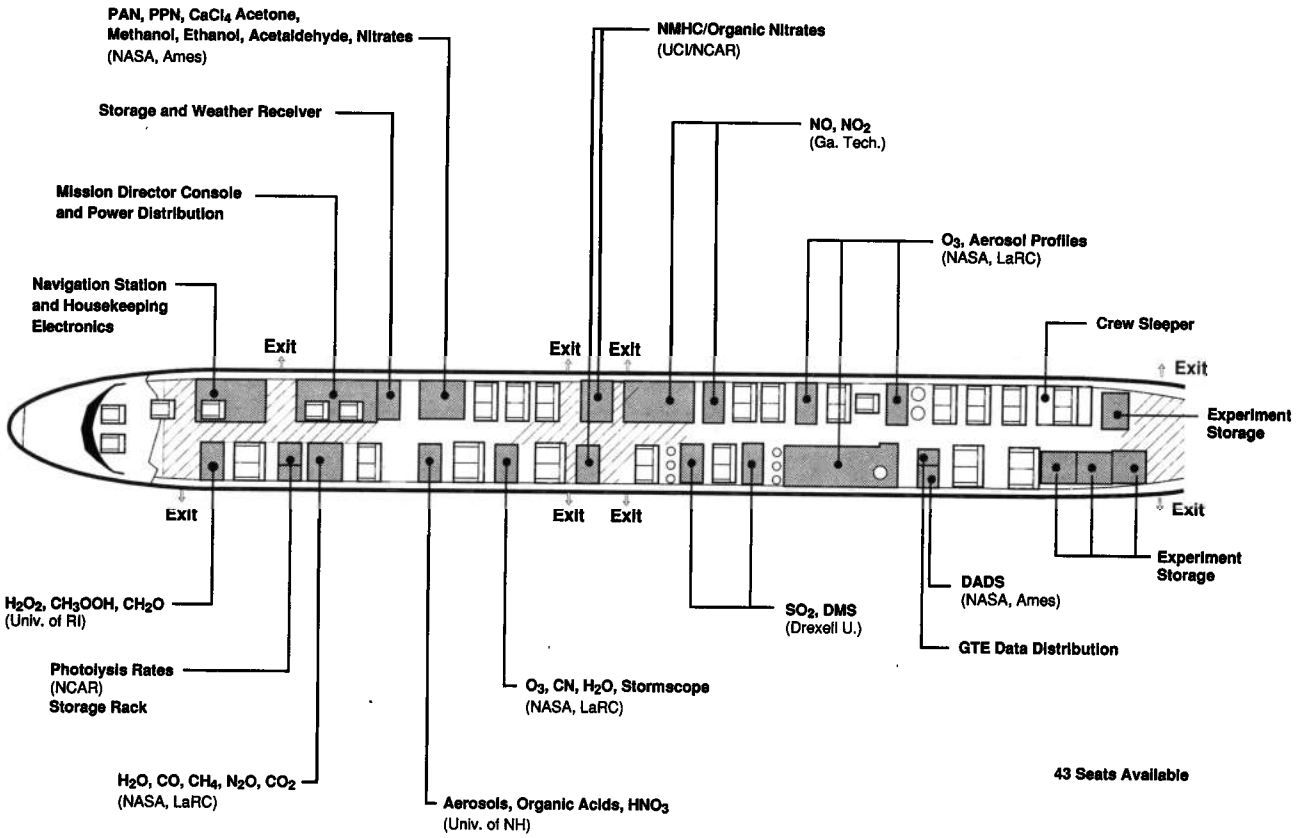

Figure 1a. Instrument layout on the NASA DC-8 aircraft during the PEM-Tropics A mission.

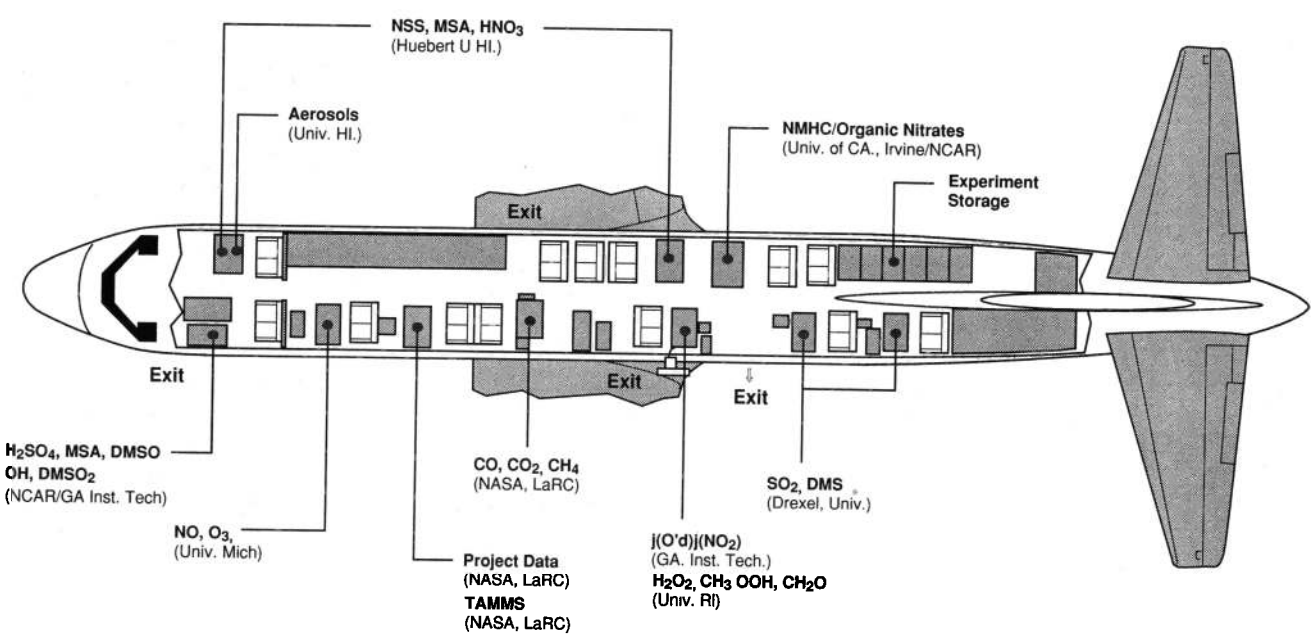

Figure 1b. Instrument layout on the NASA P-3B aircraft during PEM-Tropics A.

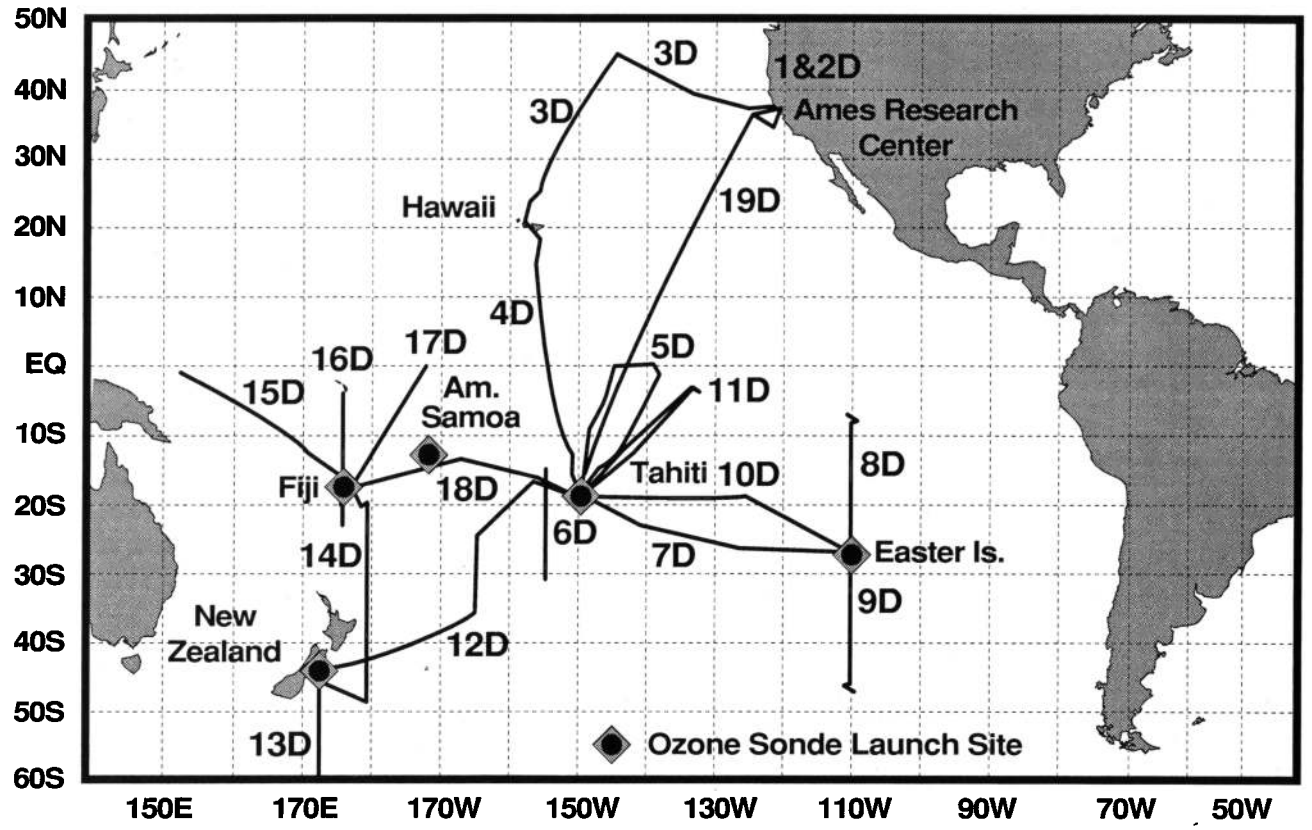

Figure 2a. Flight tracks for the DC-8 aircraft during the PEM-Tropics A campaign.

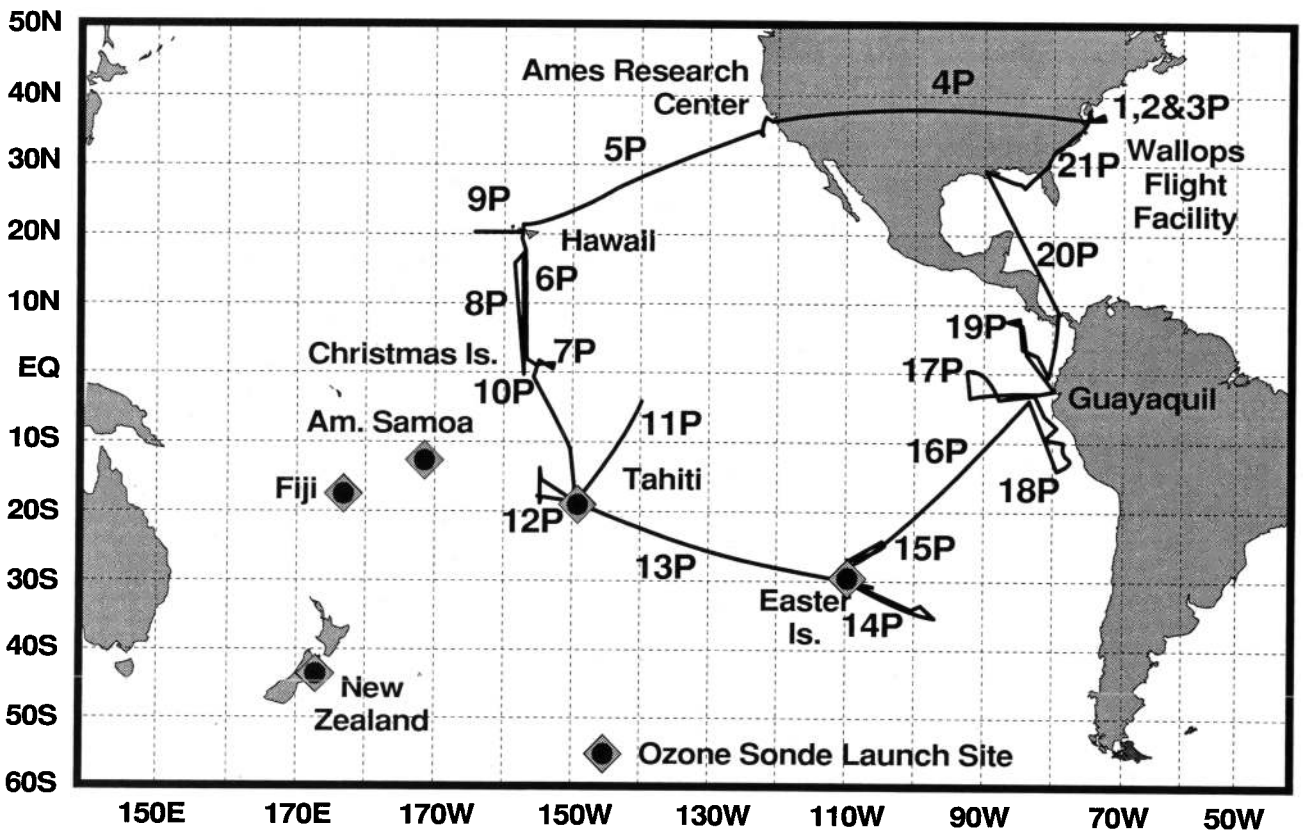

Figure 2b. Flight tracks for the P-3B aircraft during the PEM-Tropics A campaign.

Table 3a. Summary of PEM-Tropics DC-8 Aircraft Flights

Flight	State Date, UT	Start Time, UT	Stop Time, UT	Major Focus of Flight
3D	Aug. 30, 1996	1607:36	2350:00	NASA ARC to Hickam, Hawaii: latitudinal profile
4D	Aug. 31, 1996	1908:59	0435:30	Hickam, HI to Tahiti: latitudinal profile and ITCZ
5D	Sept. 3, 1996	1851:08	0320:01	Tahiti Local Flight number 1: equatorial photochemistry
6D	Sept. 5, 1996	1954:11	0325:11	Tahiti Local Flight number 2: biomass burning profile
7D	Sept. 7, 1996	1702:38	2312:00	Tahiti to Easter Island: longitudinal profile
8D	Sept. 10, 1996	1231:01	1953:28	Easter Island local flight number 1: latitudinal profile (north)
9D	Sept. 11, 1996	1603:58	2335:38	Easter Island local flight number 2: latitudinal profile (south)
10D	Sept. 14, 1996	1758:40	0011:52	Easter Island to Tahiti: longitudinal profile
11D	Sept. 16, 1996	1905:21	0257:06	Tahiti Local Flight number 3: equatorial photochemistry
12D	Sept. 18, 1996	1907:20	0448:48	Tahiti to Christchurch, New Zealand: latitudinal profile and SPCZ
13D	Sept. 21, 1996	2010:45	0617:14	Christchurch local flight: latitudinal profile (high latitudes)
14D	Sept. 23, 1996	2237:55	0628:05	Christchurch to Fiji: biomass burning and SPCZ
15D	Sept. 26, 1996	1916:38	0504:12	Fiji local flight number 1: tropical warm pool
16D	Sept. 28, 1996	2119:33	0456:16	Fiji local flight number 2: SPCZ
17D	Oct. 1, 1996	2107:48	0458:41	Fiji local flight number 3: SPCZ
18D	Oct. 3, 1996	1951:44	0327:54	Fiji to Tahiti: biomass burning/Samoa profile
19D	Oct. 5, 1996	1854:38	0341:42	Tahiti to NASA ARC: latitudinal profile

spectral radiance in 1 nm steps from 282 nm to 330 nm (UV-B region) and in 2 nm steps from 330 nm to 420 nm (UV-A region) at 30 seconds intervals. The accuracy of the actinic flux was stated as approximately ±11.5% in the UV-B and ±8% in the UV-A range. *Shetter and Müller* [this issue] report that uncertainties in the resulting photolysis frequencies for O_3, NO_2, HONO, CH_2O, H_2O_2, CH_3OOH, HNO_3, PAN, CH_3NO_3, $CH_3CH_2NO_3$, and acetone vary between ±15% and ±20%.

Aboard the P-3B, a new airborne Chemical Ionization Mass Spectrometer (CIMS) was fielded to measure OH, H_2SO_4, and MSA. Measurements reported by *Mauldin et al.* [this issue (a,b)] throughout PEM-Tropics A, and particularly for the local P-3B flight from Christmas Island (discussed in the next section), provide convincing evidence of the capability of CIMS for airborne measurement of OH and H_2SO_4.

3.2. Sulfur Photochemisty

One of the reasons for selecting Christmas Island as an operational site during PEM-Tropics A (and for the 1999 PEM-Tropics B campaign) is the almost ideal environmental conditions that exist in this region for an atmospheric sulfur photochemistry experiment. Specifically, Christmas Island is located where the prevailing meteorological conditions are relatively uniform with little, if any, anthropogenic contributions to the local sulfur budget. These conditions were highlighted in results from earlier ground-based observations [*Bandy et al.*, 1996] which showed a persistent anticorrelation between SO_2 and DMS over several diurnal cycles. The local flight from Christmas Island (P-3B flight 7P) was designed to exploit these conditions and the unique set of sulfur and photochemistry instruments aboard the P-3B aircraft.

The specific objective of the Christmas Island flights was to study the evolution of DMS oxidation chemistry in a common air mass from before sunrise through early afternoon. This was achieved using a Lagrangian sampling pattern within, and just above, the boundary layer. Simultaneous measurements of OH, DMS, SO_2, MSA (gas), H_2SO_4(gas), MS (MSA-particle), NSS, and aerosol size number distribution, as well as critical meteorological parameters, permitted one of the most intensive examinations yet of the detailed chemical processes involved in the oxidation of DMS via hydroxyl radicals. Results from this flight [*Davis et al.*, this issue] revealed distinct presunrise minima in the concentrations of OH, H_2SO_4, and SO_2 that increase to a maxima at the end of the flight in the early afternoon. Concurrent with the increase in these species was a decrease in DMS beginning near sunrise. Concentrations of OH were observed to range from sunrise values near $10^5/cm^3$ to noon time maximum values of $8\times10^6/cm^3$. *Davis et al.* [this issue] placed the overall efficiency for conversion of DMS to SO_2 for the conditions of the Christmas Island flight at 75%. This efficiency strongly supports the notion that SO_2 was the dominant precursor to H_2SO_4 in this marine environment. Equally important, these investigations showed that most of the SO_2 is converted to sulfate via heterogeneous processes as was found to be true also for the formation of MS. Using concurrent measurements of the key controlling species to constrain their model calculations, *Davis et al.* [this issue] report that the agreement between model simulations and observations for OH ranges from 5 to 20%. This

Table 3b. Summary of PEM-Tropics P-3B Aircraft Flights

Flight	State Date, UT	Start Time, UT	Stop Time, UT	Major Focus of Flight
4P	Aug. 15, 1996	0724:19	0119:55	NASA Wallops to NASA ARC
5P	Aug. 18, 1996	1817:04	0231:02	NASA-ARC to Hickam, Hawaii stratocumulus photochemistry
6P	Aug. 21, 1996	2124:12	0447:29	Hickham, HI to Christmas Island latitudinal survey and TICZ gradient
7P	Aug. 24, 1996	1434:28	2357:18	Christmas Island local flight O_3 photochemistry and sulfur oxidation cycle
8P	Aug. 26, 1996	1816:40	2306:46	Christimas Island to Hickam, HI latitudinal survey of trace gases
9P	Aug. 30, 1996	0328:59	0746:05	Hawaii local test flight
10P	Aug. 31, 1996	2015:47	0525:38	Hickam, Hawaii to Tahiti marine upwelling and latitudinal survey trace gases
11P	Sept. 3, 1996	1929:35	0359:04	Tahiti local flight number 1: marine upwelling and latitudinal survey trace gases
12P	Sept. 5, 1996	1929:11	0318:13	Tahiti local flight number 2: ozone photochemistry and latitudinal survey trace gases
13P	Sept. 7, 1996	1902:33	0248:15	Tahiti to Easter Island longitudinal survey of trace gases
14P	Sept. 10, 1996	1236:18	2013:53	Easter Island local flight number 1: latitudinal survey of trace gases
15P	Sept. 11, 1996	1806:23	0125:52	Easter Island local flight number 2: longitudinal survey and continental outflow
16P	Sept. 14, 1996	1453:05	2313:33	Easter Island to Guayaquil, Ecudaor longitudinal survey and continental outflow
17P	Sept. 18, 1996	1353:05	2151:18	Guayaquil local flight number 1: marine upwelling and continental outflow
18P	Sept. 22, 1996	1428:38	2243:20	Guayaquil local flight number 2: marine upwelling and continental outflow
19P	Sept. 23, 1996	1559:51	2314:16	Guayaquil local flight number 3: sulfur oxidation cycle and continental outflow
20P	Sept. 25, 1996	1428:11	2221:12	Guayaquil to New Orleans ITCS profiles
21P	Sept. 26, 1996	1501:44	1902:41	New Orleans to NASA Wallops

suggests that for the tropical MBL, the photochemical mechanisms in current models represent those operating in the real atmosphere.

Directly related to the sulfur/photochemical study conducted on Christmas Island are the observations of new particle formation reported by *Clarke et al.* [this issue] during three distinctly different environmental conditions. One of these, cloud outflow, is consistent with previous observations suggesting cloud outflow as a major source for aerosol nucleation. The other two environmental conditions included (1) aged and scavenged air exhibiting characteristics of long-range transport and the influence of combustion and (2) well scavenged air within the boundary layer over productive waters high in DMS. *Clarke et al.* [this issue] report that all three environments exhibited similar characteristics: low aerosol surface areas, elevated sulfuric acid, and enhanced water vapor concentrations. In the case of the MBL, *Clarke et al.* [1998] report results for a tropical MBL setting in which a nucleation event, forming new ultrafine particles was for the first time directly linked to DMS oxidation via OH through the direct observation of the intermediates SO_2 and $H_2SO_4(g)$. *Clarke et al.* [this issue] note that while the nucleation observed in the marine boundary layer may have occurred under rare conditions, it nevertheless demonstrates that nucleation can occur when surface areas are sufficiently small and concentrations of water vapor and sulfuric acid are sufficiently large.

3.3. Sulfur Distribution/Sources in the Pacific

Thornton et al. [this issue] combined measurements of SO_2 obtained during the PEM-Tropics A, the PEM-West A and B campaigns, and the First Aerosol Characterization Experiment (ACE 1) to produce a data set containing 4679 observations of SO_2 at altitudes ranging from 50 m to 12 km and covering a geographical region from 60° N to 72° S and 110° E to 80° W. This combined data set showed that in the northwestern Pacific, anthropogenic sources from eastern Asia dominate the sulfur chemistry in the lower troposphere out to distances of about 1500 km, and much farther at mid to upper troposphere altitudes, resulting in a significant gradient between the northern and southern hemispheres. Because of the absence of significant anthropogenic sources of SO_2 in the southern hemisphere, *Thornton et al.* [this issue] notes that volcanic sources from east Asia may be the dominant source of SO_2 in the mid and upper troposphere of the southern hemisphere, while DMS is a significant source of SO_2 only in the tropical marine boundary layer.

3.4. Trace Gas Distributions and Biomass Burning

An important aspect of PEM-Tropics A was to determine the extent of biomass burning influence over the remote South Pacific during the dry season of the austral tropics. The Transport and Atmoshperic Chemistry Near the Equatorial Atlantic (TRACE A) mission conducted in the same season had previously demonstrated a strong biomass burning influence over the South Atlantic, downwind of Brazil and southern Africa [*Fishman et al.* 1996]. A remarkable finding of PEM-Tropics A was the pervasiveness of biomass burning plumes and their impact on trace gases throughout the southern Pacific region. Flights from Fiji, New Zealand, Tahiti, Easter Island, and Guayaquil frequently encountered layers of biomass burning pollution in the 2–12 km column [*Gregory et al.*, this issue; *Schultz et al.*, this issue; *Talbot et al.*, this issue; *Fuelberg et al.*, this issue]. Ozone mixing ratios in these layers frequently exceeded 80 ppbv and were associated with high mixing ratios of CO and other tracers of biomass burning (C_2H_2,C_2H_6,CH_3Cl, CH_3Br). Urban pollution tracers (e.g., C_2Cl_4) were not enhanced, and hydrocarbon data indicated that these pollution layers were 1–3 weeks old. The O_3/CO enhancement ratio typically was greater than 1, consistent with chemical production of O_3 and chemical decay of CO during aging. Back trajectory analyses suggest that most of these layers originated from fires in Africa and South America and were transported to the South Pacific by strong westerly flow at subtropical latitudes [*Fuelberg et al.*, this issue], although analyses of advanced very high resolution radiometer (AVHRR) satellite images indicate that fires in Indonesia and Australia may also be sources of some of the layers [*Olson et al.*, this issue]. Of particular interest is the analysis of climatological data from 1986 to 1996 by *Fuelberg et al.* [this issue] indicating that the PEM-Tropics mission period was representative of the previous 11 years. Ozonesonde data for 1995–1997 at the PEM-Tropics sites, and earlier ozonesonde data at Samoa and New Zealand, also confirm that 1996 was not anomalous (S. J. Oltmans and J. A. Logan, private communication, 1998).

Analysis of acidic gases (e.g., HNO_3, HCOOH, and CH_3COOH) measured on the DC-8 aircraft showed that over the altitude range of 2–12 km, but particularly in the 3–7 km range, air parcels were frequently encountered within 15°–65° S latitude with mixing ratios up to 1200 pptv [*Talbot et al.*, this issue]. *Talbot et al.* [this issue] suggest the correlation of the acidic gases with CH_3Cl, PAN, and O_3 and the absence of correlation with common industrial tracer compounds such as C_2Cl or CH_3CCl_3 indicate a photochemical and biomass burning source for the plumes. *Talbot et al.* [this issue] also report that the ratio of C_2H_2/CO was typically in the 0.2–2.2 parts per trillion by volume (pptv)/ppbv range indicating relatively aged air masses in the plumes, consistent with the trajectory analysis reported by *Fuelberg et al.* [this issue].

Dibb et al. [this issue] report on the distribution of aerosol-associated soluble ions measured aboard the NASA DC-8. The authors found low mixing ratios of all ionic species throughout the free troposphere, suggesting that the soluble ions that might have been expected in air masses influenced by biomass burning had been scavenged by precipitation. They note, however, that the activity of ^7Be frequently exceeded 1000 fCi/m^3 throughout the troposphere, indicating that the scavenging of soluble ions had occurred far upwind of the DC-8 sampling region. These observations are again consistent with the trajectory analysis presented by *Fuelberg et al.* [this issue] and the chemical analysis by *Talbot et al.* [this issue] suggesting that the plumes originated from sources well west of the DC-8 sampling region. Dibb et al. also report decreasing mixing ratios of NH^{4+} with increasing altitude through out the PEM-Tropics A study area, consistent with shipboard sampling indicating strong NH_3 emissions from the equatorial Pacific. It interesting to note that observations during the P-3B flights along the west coast of South America indicated that some fresh biomass burning plumes originated from the south American continent and were transported westward by the trade winds.

An important question relative to the long-range transport of biomass burning emissions into the tropical Pacific is the impact on the general background concentrations of trace gases. Statistical analysis of the PEM-Tropics data showed that the influence of biomass burning extended beyond the plumes and pervaded the regional atmosphere, as seen, for example, in the strong positive correlation of ozone with CO found for the ensemble of PEM-Tropics data [see *McNeal et al.*, 1998, Figure 9]. A further indication of the level of enhancement for O_3 comes from the modeling analysis by *Schultz et al.* [this issue] showing that advection of ozone associated with biomass burning increases the average ozone concentration throughout the troposphere by about 7–8 ppbv. Further, during both TRACE A [*Singh et al.*, 1996] and PEM-Tropics A [*Schultz et al.*, this issue], biomass burning was found to be the dominant source of atmospheric PAN.

An interesting consequence of the layering associated with the biomass burning plumes observed in PEM-Tropics A was discussed by *Stoller et al.* [this issue]. By analyzing in situ airborne measurements obtained during PEM-Tropics A, PEM-West A and B [*Newell et al.*, 1996; *Wu et al.*, 1997], and TRACE A [*Collins et al.*, 1996], *Stoller et al.* [this issue] concluded that within the troposphere "Atmospheric layers are ubiquitous," occupying approximately one fifth of the atmospheric vertical extent sampled. During PEM-Tropics A, the most commonly observed layers exhibited characteristics of air originating from biomass burning sources. The authors note that the extensive layering observed during these GTE field missions can have an important impact on atmospheric heating, and that the rates of photochemical processes in these layers will be different from those calculated using "average" atmospheric mixing ratios.

3.5. Trace Gas Distributions

The analysis by *Gregory et al.* [this issue] illustrates the influence that convergence associated with the ITCZ and SPCZ have on chemical characteristics of their respective geographical regions. The authors analyzed in situ measurements obtained north and south of the ITCZ and the SPCZ, respectively. They report that in each region the air north and south of the respective convergence zones has distinctively different signatures indicative of the source regions. For example, the air north of the ITCZ exhibits a modest urban/industrial signature, while air south of the ITCZ and north of the SPCZ is relatively clean. Consistent with other observations reported above, the chemical signature of the air south of the SPCZ was noted to be dominated by combustion products associated with biomass burning. *Gregory et al.* [this issue] noted that the resulting chemical gradients across each zone was more pronounced below 5 km in consistent with the strong low-level convergence that is characteristic of each zone, becoming much less pronounced at higher altitudes. Back trajectory analysis by the FSU group [*Fuelberg et al.*, this issue] also showed that much of the tropical air having low ozone mixing ratios originated east of the observation region and had not passed over land masses for at least 10 days.

Measurements of CO_2 on the DC-8 and P-3B during PEM-Tropics A resulted in the most extensive aerial CO_2 data set re-

corded over the South Pacific basin. *Vay et al.* [this issue] analyzed PEM-Tropics A flight data combined with CO_2 surface measurements from NOAA/CMDL and NIWA to establish vertical and meridional gradients for the region. They conclude that the observed CO_2 distributions in the south tropical Pacific were noticeably affected by interhemispheric transport with northern air masses depleted of CO_2 frequently observed south of the ITCZ. *Vay et al.* [this issue] note that regional processes also modulated background concentrations as large-scale plumes from biomass burning activities produced enhanced CO_2 mixing ratios within the lower to mid troposphere over portions of the remote Pacific. Of particular interest was a shift in the location of an apparent equatorial CO_2 source observed in the surface data between 15° N and 15° S, but realized in the airborne data between 8° N and 8.5° S, demonstrating the importance of vertical trace gas profiles in potential source/sink regions as they provide an additional constraint for global scale trace gas budget models.

Measurements of gas phase hydrogen peroxide (H_2O_2) and methylhydroperoxide (CH_3OOH) aboard the DC-8 and P-3B aircraft have also provided an extensive data set covering the region from 70° S to 60° N and 110° E to 80° W in the Pacific and 40° S to 15° N and 45° W to 70° E in the South Atlantic over an altitude range from 76 m to 13 km. *O'Sullivan et al.* [this issue] reports that both of these compounds exhibited a maximum concentration at a given altitude along the equator and decreasing in concentration with increasing latitude in the southern and northern hemisphere. Similar to the chemical gradients reported by *Gregory et al.* [this issue], *O'Sullivan et al.* [this issue] notes that the latitude gradient above 4 km is substantially reduced and at altitudes above 8 km there is no latitudinal dependency.

3.6. Photolysis Frequences

Calculated photolysis rate coefficients, that is, J values, are key parameters in photochemical models. In past GTE campaigns, clear-sky model-calculated J values have been adjusted for cloud effects based on differences between calculated $J(NO_2)$ and $J(NO_2)$ derived from Eppley radiometers. However, a continuing cause of concern has been the large systematic changes in the clear-sky baseline for the Eppley radiometers between previous campaigns (e.g., as great as a factor of 1.5). This prompted a detailed comparison of several radiometric determinations of $J(NO_2)$ during PEM-Tropics A, discussed in detail by *Crawford et al.* [this issue]. As noted earlier, a new actinic flux spectroradiometer system was flown aboard the DC-8 aircraft [*Shetter and Müller*, this issue] to measure the actinic flux values needed to calculate J values. Also aboard the DC-8 were zenith and nadir viewing $J(NO_2)$ filter radiometers (see Table 1a). Aboard the P-3B, solar flux measurements were obtained using zenith and nadir viewing Eppley radiometers (see Table 1b).

The only period during PEM-Tropics A where the two aircraft were sufficiently close geographically and temporally to permit comparison of all three radiometric techniques was during flights 4D (DC-8) and 10P (P-3B) in the marine boundary layer near Christmas Island. During this period, the three radiometers exhibited trends consistent with each other and with model calculations. However, they disagreed in magnitude with the $J(NO_2)$ filter radiometers being approximately 30% greater than the spectroradiometers and the Eppley radiometers falling between the $J(NO_2)$ and the spectroradiometers. Across all DC-8 flights, agreement between the $J(NO_2)$ filter radiometers and spectroradiometers was exceptional with regard to the variation in $J(NO_2)$ due to clouds (i.e., R^2=0.98). The $J(NO_2)$ filter radiometers, however, continued to be consistently higher than the spectroradiometers by 30%. *Crawford et al.* [this issue] note that while model calculations agreed best with values from the spectroradiometer, the accuracy of $J(NO_2)$ cannot be assured to better than within 30%.

Since each technique appears to accurately capture the variability in $J(NO_2)$ due to clouds, the recommendation of these findings has been to normalize the variations to the clear-sky baseline of the model calculations. Although, this does not improve the accuracy of photochemical model calculations, it does ensure a consistent baseline for J values that permits comparisons of photochemical calculations between GTE campaigns that are free of any systematic biases introduced by changes in the radiometer baselines.

A secondary finding based on spectroradiometer measurements of $J(NO_2)$ and $J(O^1D)$ suggests that the two J values exhibit roughly equivalent responses to clouds. This confirms that correcting all model calculated J values based on the cloud response of $J(NO_2)$ should not be considered a large source of uncertainty in model calculations.

3.7. Ozone Photochemistry

A major objective of the PEM and TRACE-A missions has been to improve understanding of O_3 production and loss in the remote troposphere. As noted above, comparisons by *Schultz et al.* [this issue] using the PEM-Tropics A measurements of NO and NO_2 reported from the PF-TP-LIF system reproduced the modeled ratio to within 30%, with similar success in simulating concentrations of peroxides. These results are important since they indicate that key aspects of photochemical processes in the troposphere are understood. Model evaluation of the photochemical ozone budget over the South Pacific [*Schultz et al.*, this issue] revealed that the tropical Pacific is a net photochemical sink. Specifically, chemical production was found to balance only half of photochemical loss. On the basis of the ratio (delta O_3) /(delta CO), O_3 transport from biomass burning regions was found to be significant in balancing the remaining photochemical loss. Photochemical production in the lower troposphere was also found to be largely driven by NO_x derived from the decomposition of PAN that was transported from biomass burning regions.

Photochemical model analysis of the PEM-Tropics A data has reinforced a scenario that has emerged from previous GTE missions about the factors controlling O_3 in the tropical troposphere. In this picture, which is markedly different from the prevailing view of 20 years ago, tropospheric NO_x levels are sufficiently high that O_3 concentrations in the tropical troposphere are determined by a balance between in situ photochemical production and loss. As a result, photochemical production of ozone dominates the stratospheric flux in controlling column O_3 density. Stratospheric intrusions are dramatic local events that strongly impact the local tropospheric ozone column density. However, the photochemical production of O_3 on a global scale, driven by NO_x from natural and anthropogenic sources, ultimately dominates the tropospheric O_3 budget [*Schultz et al.*, this issue; *Crawford et al.*, 1997a, b; *Davis et al.*, 1996; *Jacob et al.*, 1996]. Changes in NO_x emissions in the tropics as a result of industrialization and changes in biomass burning practices would have a major impact on O_3 in the tropical troposphere and, hence, the global oxidizing power of the atmosphere.

4. Concluding Remarks

The PEM-Tropics A mission provided the first detailed survey of tropospheric ozone and sulfur chemistry over the South Pacific.

It complements previous GTE missions conducted in other regions of the tropics (ABLE 2A and 2B, CITE 3, PEM-West A and B, TRACE A). The observations from PEM-Tropics A showed that seasonal biomass burning in the southern tropics causes major enhancements in background concentrations of ozone and other gases over the most remote regions of the South Pacific atmosphere. From this result it appears that the biomass burning perturbation to atmospheric composition is global in scale, with major implications for the global oxidizing power of the atmosphere. Another important finding of PEM-Tropics A was that the South Pacific Convergence Zone (SPCZ) represents a major barrier to atmospheric transport, and acts in combination with the ITCZ to define boundaries for air masses over the tropical Pacific. Focused studies of sulfur chemistry conducted in PEM-Tropics A demonstrated a diurnal evolution of DMS-SO_2-H_2SO_4-OH consistent with results from photochemical models, and observed for the first time episodes of new particle formation in the marine boundary layer. Finally, the PEM-Tropics A mission featured many improvements in critical instrumentation for tropospheric chemistry including sub-pptv measurement of NO, high-quality measurements of NO_2, OH, and H_2SO_4, and spectroradiometer measurements.

The PEM-Tropics B mission to be conducted in March–April 1999 will conclude the PEM mission series by surveying the atmosphere over the South Pacific during the wet season of the southern tropics. The objectives of PEM-Tropics B extend beyond those of PEM-Tropics A to include focused studies of HO_x chemistry, of the large-scale ozone minimum in the western equatorial Pacific, and of vertical transport by deep convection in the ITCZ and the SPCZ. Biomass burning influence on ozone should be near its seasonal minimum during the PEM-Tropics B period, while lightning influence should be near its seasonal maximum. Data for ozone over the South Pacific indicate particularly low concentrations in March–April [*Fishman et al.*, 1990; *Johnson et al.*, 1990; *Oltmans and Levy*, 1994]. The continuous ozonesonde network operated as part of PEM-Tropics indicates low ozone concentrations throughout the tropospheric column in March–April, with none of the high-ozone layers found in September–October. Some anthropogenic pollution could still be transported to the South Pacific during PEM-Tropics B by the circulation of Asian outflow around the Pacific High. Some interhemispheric transport of biomass burning pollution from the northern tropics is also possible. In any case, considerable contrast should be found with the conditions observed in PEM-Tropics A.

Acknowledgments. The PEM-Tropics A expedition would not have been successfully conducted without the cooperation, support, and collaboration of personnel and colleagues from organizations both foreign and domestic. Many exhibited a personal interest in our endeavors and performed well beyond the normal call of duty. We give special thanks to Patrick Simon, Isabelle Leleu, and colleagues at Meteo France in Tahiti. Without their dedicated efforts prior to our arrival in Tahiti, and patience during our operations in Tahiti, the PEM-Tropics A mission would not have been possible. In addition, we owe a special thanks to the DC-8 and P-3B personnel. Their dedication and patience were a critical element in translating the, often, unrealistic desires of the PEM-Tropics A science team into reality. Finally, we express thanks to Mike Cadena and Fred Reisinger in the GTE contractor Project office for their dedicated support in the "care and feeding" of the science team during the field deployment.

References

Bandy A. R., D. C. Thornton, B. W. Blomquist, S. Chen, T. P. Wade, J. C. Ianni, G. M. Mitchell, and W. Nadler, Chemistry of dimethyl sulfide in the equatorial Pacific atmosphere, *Geophys. Res., Lett., 23*, 741–744, 1996.

Bradshaw, J., D. Davis, J. Crawford, G. Chen, R. Shetter, M. Muller, G. Gregory, G. Sachse, J. Barrick, D. Blake, B. Heikes, H. Singh, J. Mastromarino, and S. Sandholm, Photofragmentation two-photon laser-induced dectection of NO_2 and NO: comparison of measurements with model results based on airborne observations during PEM-Tropics A, *Geophys. Res. Lett.*, in press, 1999.

Browell E. V., et al., Ozone and aerosol distributions and air mass characteristics over the South Atlantic basin during the burning season (Paper 95JD02536), *J. Geophys. Res., 101*, 24,043–24,068, 1996.

Clarke, A. D., F. Eisele, V. N. Kapustin, K. Moore, R. Tanner, L. Mauldin, M. Litchy, B. Lienerts, M. A. Carroll, and G. Albercook, Nucleation in the equatorial free troposphere: Favorable environments during PEM-Tropics, *J. Geophys. Res.*, this issue.

Clarke, A. D., et al., Particle nucleation in the tropical boundary layer: A case study involving marine sulfur sources, *Science*, in press, 1998.

Collins, J. E., Jr., B. E. Anderson, G. W. Sachse, J. D. W. Barrick, L. O. Wade. L. G. Burney, and G. F. Hill, Atmospheric fine structure during GTE TRACE A: Relationships among ozone, carbon, and water vapor, *J. Geophys. Res., 101*, 24,307–24,316, 1996.

Crawford, J., et al., Photostationary state analysis of the NO_2NO system based on airborne observations from the western and central North Pacific, *J. Geophys. Res., 101*, 2053–2072, 1996.

Crawford, J. H., et al., An assessment of ozone photochemistry in the extratropical western North Pacific: Impact of continental outflow during the late winter/early spring, *J. Geophys. Res., 102*, 28,469–28,488, 1997a.

Crawford, J. H., et al., Implications of large scale shifts in tropospheric NO_x levels in the remote tropical Pacific, *J. Geophys. Res., 102*, 28,447–28,468, 1997b.

Crawford, J., et al., D. Davis, G. Chen, R. Shetter, M. Müller, J. Barrick, and J. Olson, An assessment of cloud effects on photolysis rate coefficients: Comparison of experimental and theoretical values, *J. Geophys. Res.*, this issue.

Davis, D. D., Project GAMETAG: An overview, *J. Geophys. Res.*, 85, 7285–7292, 1980.

Davis, D., et al., Assessment of the ozone photochemistry tendency in the western North Pacific as inferred from PEM-West A observations during the fall of 1991, *J. Geophys. Res., 101*, 2111–2134, 1996.

Davis, D. D., et al., DMS oxidation in the equatorial Pacific: Comparison of model simulations with field observations for DMS, SO_2, H_2SO_4(gas), MSA(gas), MS, and NSS, *J. Geophys. Res.*, this issue.

Dibb, J.E., R.W. Talbot, E.M. Scheuer, D.R. Blake, N. J. Blake, G. L. Gregory, G. W. Sachse, and D.C. Thornton, Aerosol chemical composition and distribution during the Pacific Exploratry Mission, Tropics, *J. Geophys. Res.*, this issue.

Drummond, J. W., D. H. Ehhalt, and A. Volz, Measurements of nitric oxide between 0–12 km altitude and 67° N–60° S latitude obtained during STRATOZ III., *J. Geophy. Res., 93*, 15,831–15,849, 1988.

Eisele, F. L., and D. J. Tanner, Ion-assisted tropospheric OH measurements, *J. Geophys. Res.*, 96, 9295–9308, 1991.

Fishman, J., C.E. Watson, J.C. Larsen, and J.A. Logan, Distribution of tropospheric ozone determined from satellite data, *J. Geophys. Res., 95*, 3599–3617, 1990.

Fishman, J., J. M. Hoell Jr., R. J. Bendura, R. J. McNeal, and V. W. J. H. Kirchhoff, NASA GTE TRACE A experiment (September–October 1992): Overview, *J. Geophys. Res., 101*, 23,865–23,880, 1996.

Fuelberg, H. E., R. E. Newell, S. Longmore, Y. Zhu, D. J. Westberg, E. V. Browell, D. R. Blake, G. R. Gregory, and G. W. Sache, A meteorological overview of the PEM-Tropics Periods, *J. Geophys. Res.*, this issue.

Gregory, G. L., et al., Chemical characteristics of pacific, tropospheric air in the region of the ITCZ and SPCZ, *J. Geophys. Res.*, this issue.

Hoell, J. M., D. D. Davis, S. C. Liu, R. Newell, M. Shipham, H. Akimoto, R. J. McNeal, R. J. Bendura, and J. W. Drewry, Pacific Exploratory Mission-West A (PEM-West A): September–October 1991. *J. Geophys. Res., 101*, 1641–1653, 1996.

Hoell, J. M., D. D. Davis, S. C. Liu, R. E. Newell, H. Akimoto, R. J. McNeal, and R. J. Bendura, Pacific Exploratory Mission-West B (PEM-West B): February–March 1994. *J. Geophys. Res., 102*, 28,223–28,239, 1997.

Jacob, D. J., et al., Origin of ozone and NO_x in the tropical troposphere: A photochemical analysis of aircraft observations over the South Atlantic basin, *J. Geophys. Res., 101*, 24,235–24,350, 1996.

Johnson, J. E., R. H. Gammon, J. Larsen, T. S. Bates, S. J. Oltmans, and J. C. Farmer, Ozone in the marine boundery layer over the Pacific and Indian Oceans: Latitudinal gradients and diurnal cycles, *J. Geophys. Res., 95*, 11,847–11,856, 1990.

Mauldin, R. L., III, D. J. Tanner, and F. L. Eisele, Measurements of OH during PEM-Tropics A, *J. Geophys. Res.*, this issue (a).

Mauldin, R. L., III, D. J. Tanner, J. A. Heath, B. J. Huebert, and F. L. Eisele, Observations of H_2SO_4 and MSA during PEM-Tropics, *J. Geophys. Res.*, this issue (b).

McNeal, R. J., D. J. Jacob, D. D. Davis, and S. C. Liu, The NASA Global Tropospheric Experiment: Recent accomplishments and future plans, IGACtiv. NewsL., *13*, 2–18, 1998.

Newell, R. E. , Z.-X. Wu, Y. Zhu, W. Hu, E. V. Browell, G. L. Gregory, G. W. Sachse, J. E. Collins Jr., K.. K. Kelly, and S. C. Liu, Vertical fine-scale atmospheric structure measured from the NASA DC-8 during PEM-West A, *J. Geophys. Res.*, *101*, 1943–1960, 1996.

Olson, J., B. Baum, D. Cahoon, and J. Crawford, "The frequency and distribution of forest, savanna, and crop fires over torpical regions during PEM-Tropics A," *J. Geophys. Res.*, this issue.

O'Sullivan, D. W., B. G. Heikes, M. Lee, W. Chang, G. Gregory, D. Blake, and G. Sachse, The distribution of hydrogen peroxide and methylhydroperoxide in the Pacific and South Atlantic Oceans, *J. Geophys. Res.*, this issue.

Sandholm, S., S. Smyth, R. Bai, and J. Bradshaw, Recent and future improvements in two-photon laser-induced fluorescence NO measurement, *J. Geophys. Res.*, *102*, 28,651–28,662, 1997.

Schultz, M., et al., On the origin of tropospheric ozone and NO_x over the tropical South Pacific, *J. Geophys. Res.*, this issue.

Shetter, R. E., and M. Müller, Photolysis frequency measurements using actinic flux spectroradiometry during the PEM-Tropics mission: Instrumentation description and results, *J. Geophys. Res.*, this issue.

Singh, H., et al., Reactive nitrogen and ozone over the western Pacific: Distribution, partitioning, and sources, *J. Geophys. Res.*, *101*, 1793–1808, 1996.

Stoller, P., et al., Measurements of atmospheric layers from the NASA DC-8 and P-3B aircraft during PEM-Tropics A, *J. Geophys. Res.*, this issue.

Talbot, R. W., J. E. Dibb, E. M. Scheuer, D. R. Blake, N. J. Blake, G. L. Gregory, G. W. Sachse, J. D. Bradshaw, S. T. Sandholm, and H. B. Singh, Influence of biomass combustion emissions on the distribution of acidic trace gases over the southern Pacific basin during austral springtime, *J. Geophys. Res.*, this issue.

Thornton, D. C., A. Bandy, B. Bloomquist, A. Driedger, and T. Wade, Sulfur dioxide distributions over the Pacific Ocean 1991–1996. *J. Geophys. Res.*, this issue.

Vay, S. A., B. E. Anderson, T. J. Conway, G. W. Sachse, J. E. Collins Jr., D. R. Blake, and D. J. Westberg, Airborne observations of the tropospheric CO_2 distribution and its controlling factors over the South Pacific basin, *J. Geophys. Res.*, this issue.

Wu, Z.-X., R. E. Newell, Y. Zhu, B. E. Anderson, E. V. Browell, G. L. Gregory, G. W. Sachse, and J. E. Collins Jr., Atmospheric layers measured from the NASA DC-8 during PEM-West B and comparison with PEM-West A, *J. Geophys. Res.*, *102*, 28,353–28,365, 1997.

R. J. Bendura, J. M. Hoell, and J. L. Raper, NASA Langley Research Center, Hampton, VA 23681-0001. (e-mail: j.m.hoel@larc.nasa.gov)

D. D. Davis and M. O. Rodgers, Georgia Institute of Technology, Atlanta, GA 30332.

H. E. Fuelberg, Florida State University, Tallahassee, FL 32306.

D. J. Jacob, Harvard University, Cambridge, MA 02138.

R. J. McNeal, NASA Headquarters, Washington, DC 20546.

R. E. Newell, Massachusetts Institute of Technology, Cambridge, MA 02139.

(Received July 1, 1998; revised October 13, 1998;
accepted November 10, 1998.)